Cardiomyocyte sarcomere length variability: Membrane fluorescence versus second harmonic generation myosin imaging

Oleg Lookin, Pieter de Tombe, Najlae Boulali, Csilla Gergely, Thierry Cloitre, Olivier Cazorla

Cardiomyocyte Sarcomere Length Variability: membrane fluorescence versus second harmonic generation myosin imaging.

Oleg Lookin [1!], Pieter de Tombe [2,3!], Najlae Boulali [2], Csilla Gergely [4], Thierry Cloitre [4], and Olivier Cazorla[2*]

1 Institute of Immunology and Physiology, Ural Branch of Russian Academy of Sciences, Yekaterinburg, Russia.

2 Laboratory "Physiologie et Médecine Expérimentale du Coeur et des Muscles", Phymedexp, INSERM – CNRS - Montpellier University, Montpellier, France.

3 Physiology and Biophysics, University of Illinois at Chicago, Chicago, IL 60612, USA

4 L2C, University of Montpellier, CNRS, Montpellier, France.

! equal contribution

Keywords: fluorescent microscopy, second-harmonic generation, sarcomere length

Running title: Cardiac sarcomere length variability.

* Correspondence to:

Olivier CAZORLA

PhyMedExp, Université de Montpellier, INSERM, CNRS,

CHU Arnaud de Villeneuve, 34295 Montpellier, France

Phone: +33 467 41 52 44; Fax: +33 467 41 52 42

olivier.cazorla@inserm.fr

ABSTRACT

Sarcomere length (SL) and its variation along the myofibril strongly regulate integrated coordinated myocyte contraction. It is therefore important to obtain individual SL properties. Optical imaging by confocal fluorescence (for example using ANEPPS) or transmitted light microscopy is often used for this purpose. However, this allows for visualization of structures related to Z-disks only. In contrast, second harmonic generation (SHG) microscopy visualizes A-band sarcomeric structures directly.

Here we compared averaged SL and its variability in isolated relaxed rat cardiomyocytes by imaging with ANEPPS and SHG. We found that SL variability, evaluated by several absolute and relative measures, is two times smaller using SHG *vs* ANEPPS, while both optical methods give the same average (median) SL.

We conclude that optical methods with similar optical spatial resolution provide valid estimations of average SL but the use of SHG microscopy for visualization of sarcomeric A-bands may be the “gold standard” for evaluation of SL variability, due to absence of optical interference between the sarcomere center and non-sarcomeric structures. This contrasts with sarcomere edges where t-tubules may not consistently colocalize to Z-disks. The use of SHG microscopy instead of fluorescent imaging can be a prospective tool to map sarcomere variability both in vitro and in vivo conditions and to reveal its role in the functional behavior of living myocardium.

SUMMARY

Cardiomyocyte sarcomere length variability assessed by second harmonic generation (SHG) was significantly less than by ANEPPS confocal fluorescence. We conclude that

SHG derived SL variability may reflect the true relaxed myocyte sarcomeric ultra-structure.

INTRODUCTION

Sarcomeres are the basic contractile elements in a striated muscle cell. The actual sarcomere length (SL), the inherent properties of individual sarcomeres, and the mechanical inter-communication between adjacent sarcomeres are important for the whole-cell contractile response, both in cardiac (Dobesh et al., 2002; de Tombe and ter Keurs, 2016) and skeletal muscle (Herzog, 2022). The ability to characterize SL under certain conditions (ambient, mechanical, etc) makes it possible to conclude how changes in sarcomere length are linked to functional behavior of the cardiomyocyte.

Optical imaging is the only available tool for characterizing the sarcomeric striation pattern and the corresponding average SL, which is highly informative for understanding the functional relationships between actual SL and contractile state of the cell (Bub et al., 2010; Botcherby et al., 2013; Aguirre et al., 2014; Guo and Song, 2014; Pasqualin et al., 2016; Kobirumaki-Shimozawa et al., 2018; Varga et al., 2020; Dowrick et al., 2021). Recent studies have also focused on the existence of intracellular SL heterogeneity in striated muscle (Rassier, 2017; Haeger et al., 2020; Adkins et al., 2022) and, importantly, its alteration upon the transition of myofilaments from the inactivated to the activated state (Johnston et al., 2016; de Souza Leite et al., 2017; Moo et al., 2017; Haeger and Rassier, 2020; Lookin et al., 2022). Therefore, special care is needed to choose a proper method for SL measurements.

For many years, the use of membrane staining by fluorescent dyes (particularly of the ANEPPS family) has been an extensively used approach (Bub et al., 2010; Guo and Song, 2014; Wagner et al., 2014; Yue et al., 2017). These labeling dyes, however, only visualize membrane invaginations, the t-tubules, but not directly the internal cellular

components that compose the sarcomeres. As a result, relying on a membrane dye may render proper determination of the location of the sarcomeric Z-disk somewhat uncertain. This limitation may be overcome by employing genetically encoded fluorescent sarcomeric proteins that are introduced by viral infection techniques. For example, fluorescent labeling of α-actinin has been used to visualize sarcomeric Z-disks (Shintani et al., 2014; Tsukamoto et al., 2016; Kobirumaki-Shimozawa et al., 2016; Kobirumaki-Shimozawa et al., 2018). However, both the fluorescent labeling and the viral infection delivery methods involve introduction of “non-natural” compounds into the living cell that may affect function and structure of the cardiac myocyte.

Second-harmonic generation (SHG) microscopy is, by design, a label free imaging modality that has been highly effective in the examination of cellular structures in intact living tissues (Recher et al., 2009; Buttgereit, 2017). In addition to high-contrast optical sections of cells and tissues, SHG imaging can also provide detailed structural information. This technique has been successfully employed to visualize sarcomeres (Garcia-Canadilla et al., 2014; Zhao et al., 2019; Varga et al., 2020; Homan et al., 2021) and, therefore, is specifically suited to the study of SL variability. SHG-based images of myocytes have revealed that the source of the SHG signal from the sarcomere are the myosin tails that assemble into a rod structure forming the central core of thick myosin filaments (Plotnikov et al., 2006).

Because t-tubule visualization is often used for the determination of average SL, we aimed here to compare the characteristics of individual SL populations as obtained by the two principally different optical methods: second harmonic generation (SHG) and t-tubular fluorescent labeling (ANEPPS).

METHODS

All investigations conformed to European Parliament Directive 2010/63/EU and approved by the ethics committee “Comité d’éthique pour l’expérimentation animale Languedoc-Roussillon”.

Isolated cardiomyocytes

Intact cardiomyocytes were isolated from the heart by enzymatic digestion as previously described (Andre et al., 2010). Briefly, the heart was harvested from deeply anesthetized male rats (pentobarbital 50mg/kg) while beating, quickly cannulated on a Langendorff apparatus, and perfused with a physiological solution at 37°C via the aorta. This solution contained (in mM): NaCl 117, KCl 5.7, $NaHCO_3$ 4.4, KH_2PO_4 1.5, $MgCl_2$ 1.7, HEPES 21, glucose 11, taurine 20, pH = 7.2 adjusted with NaOH. The heart was first washed with this calcium (Ca^{2+})-free extracellular physiological solution and then with an enzyme-containing solution (1.25 mg/ml Collagenase type IV, Worthington) during 25 to 35 minutes. The left and right ventricles were separated, and digestion was stopped with bovine sodium albumin. The tissue was then mechanically disrupted with a pipette to release the myocytes. The extracellular Ca^{2+} concentration was progressively increased to 1 mM. All subsequent experiments were performed using a modified Tyrode solution (in mM): NaCl 140, KCl 4, $MgCl_2$ 1, HEPES 20, $CaCl_2$ 0.1, glucose 11, pH = 7.4 at room temperature. Myocytes were not electrically stimulated and 20 mM BDM was added to all solutions to prevent spontaneous contractile activity.

The analysis of intracellular variability in sarcomere lengths was performed using second harmonic generation microscopy measurements (SHG) + fluorescent

measurements with membrane staining by di-4-ANEPPS (ANEPPS) for fully relaxed and non-stretched cardiomyocytes (*n* = 26 from *N* = 3 hearts).

Optical measurements

Just prior to the start of the SHG/ANEPPS measurements, cardiomyocytes were labeled with the fluorescent dye di-4-ANEPPS as follows: 0.2 μL of ANEPPS (1 mM DMSO stock solution) was added to 1 mL of cell suspension in Tyrode solution at room temperature. Following sedimentation during the 10-minute dye treatment, the supernatant was removed and replaced by 3 mL fresh dye-free Tyrode. An aliquot of cells was placed in ~1 ml fresh modified Tyrode solution in a glass bottomed 35 mm plastic petri dish (room temperature). SHG images were then recorded using a custom-made multiphoton microscope setup based on a Tsunami tunable Ti:Sapphire laser (Spectra-Physics) and an upright SliceScope microscope (MPSS-1000P) furnished with a multiphoton galvanometer scan head (MP-2000) both from Scientifica (Varga et al., 2020). The Ti-Sa laser was operated in pulsed mode configuration for sample excitation, 875 nm wavelength, 80 MHz frequency and ~100 fs pulse duration. A Nikon CFI75 LWD-16x-W objective (NA 0.8, water immersion) was used to focus the laser beam onto the myocyte. The SHG signal was recorded by a 1.4-NA water-immersion condenser (U-AAC, Olympus), through a 482 nm long-pass dichroic mirror (86-331, Edmund Optics) and a 447 nm high-performance 60 nm band-pass filter (48-074, Edmund Optics) and then detected by a H7422P photomultiplier (Hamamatsu). Epi-fluorescence two-photon images were recorded using a 735 nm long-pass dichroic mirror, followed by sequential short-pass/long-pass filters to form a 450 nm to 750 nm bandpass filter, 1024x1024 ~150 nm XY scan pixel size, and then detected by a R928P photomultiplier (Hamamatsu). Several consecutive scans (~10 frames) of the same cell position were recorded to increase signal-to-noise ratio during further off-line image

post-processing. In a subset of experiments, images were acquired at 5 separate Z-slices, ranging approximately from the top to the bottom of the isolated myocyte (cf. Figure 4).

Analysis of variability in sarcomere lengths

The analysis of variability in individual sarcomere lengths was implemented by custom-made software EqapAll6 (developed by Oleg Lookin). For each cell in the SHG/ANEPPS measurements, we used the two optical images separately for SHG (to reveal the regularity of sarcomeric A-bands) and for ANEPPS (to reveal the regularity of t-tubular invaginations of cell membrane). By design, the two images were always aligned to each other and five regions of interest (ROI) with the same positions, sizes, and angles were used for each image (Fig. 1A). In all measurements, the ROIs were placed to cover as much area of a cell as possible, but their lengths and angles were set to follow a straight part of myofibrils. Curved myofibrils, crossing myofibrils or myofibrils with irregular staining along their length were omitted from the selection.

The lengths of individual sarcomeres were determined using an algorithm based on analysis of the sarcomere striation profile. For this algorithm, the input data were the sarcomere striation profiles obtained for each ROI. The positions of sarcomere edges in ANEPPS measurements were found from the local maxima in the sarcomere striation profile. In contrast, the local maxima in the sarcomere striation profile in SHG measurements reflected the positions of sarcomere centers. To test if the use of local maxima or minima in the same striation profile can produce a difference in SL variability, we also compared the data of SHG/ANEPPS measurements using both local extrema (cf. Fig. 3). The individual SL sets obtained for each ROI were then combined to increase the resulting number of individual SLs prior to the analysis of their variability.

An expanded view of striation profiles obtained for the same ROI using SHG/ANEPPS measurement is shown in Fig. 1B. Note that the local maxima in these two striation profiles are shifted relative to each other by a half sarcomere, as indicated by the arrows in Fig. 1B. The local maxima in the SHG measurement correspond to the centers of A-bands, while the local maxima in the ANEPPS measurement index the local peak intensity of t-tubule staining that putatively corresponds to the position of sarcomeric Z-disks.

Statistical analysis

Statistical analysis was carried out with GraphPad Prism 9.3.1 (GraphPad Software). Because some of the individual SL sets did not follow the normal shape, we analyzed median SL values as well as the absolute and relative measures of variability applicable for non-normal data samples. The evaluation of significance in the median SL values as well as the absolute/relative measures of SL variability between SHG and ANEPPS was implemented by the Wilcoxon matched pairs signed rank test. Differences were considered significant at $p < 0.05$. Data are presented as mean ± S.D.

RESULTS

We analyzed the variability of individual sarcomere lengths (SLs) using SHG imaging to solely and directly visualize sarcomeric A-bands. For comparison, simultaneous ANEPPS fluorescence was used to visualize t-tubule structures. Median values of SL as well as absolute and relative measures of SL variability were analyzed and contrasted between these two image modalities. The averaged median SL values were not significantly different between the two optical measurements (p = 0.901, Fig. 2A). In contrast, the absolute and relative measures of variability of individual sarcomere lengths were sensitive to the method of measurements. The absolute measures of SL variability – inter-quartile range and median absolute deviation – were ~two-fold higher for SL measurements using ANEPPS *vs* SHG (the difference is significant at $p < 0.0001$ for any measure, Fig. 2B-C). For example, the median absolute deviation of SL was found to be 0.04 ± 0.02 μm in SHG *vs* 0.09 ± 0.02 μm in ANEPPS measurements (Fig. 2C). Likewise, the relative measures of SL variability – inter-quartile range divided by median SL value or median absolute deviation divided by median SL value – were significantly higher (~2.0-2.2 fold) for ANEPPS *vs* SHG (difference is significant at $p < 0.0001$ for each measure, Fig. 2D-E). The higher SL variability obtained by ANEPPS measurements is demonstrated by plotting superimposed SL distributions averaged for all SHG and ANEPPS measurements (Fig. 2F). Each plot peaks at averaged median SL and shows how much the SL values are distributed (as a % of the median SL value). The distribution for ANEPPS measurements is roughly two times wider than the distribution for SHG measurements.

The calculation of sarcomere length using ANEPPS measurement was based on the determination of local maxima in the intensity profiles that correspond to the peak

intensities of the individual t-tubules. Instead, we can use local minima to check whether their positions correlate with the local maxima of the SHG measurement (A-band centers). We did not find any difference between these two approaches, that is, in the ANEPPS measurement the spreads of local maxima (the physical presence of t-tubules) and local minima (the interval between two adjacent t-tubules) were quantitatively similar. The plots of spread range of median SL values and median absolute deviation divided by median SL values, as obtained for SHG and ANEPPS measurements by using of local maxima or local minima as index for determining the local SL, are shown in Fig. 3. Median SL values were found to be insensitive to the method of optical measurement or the selection of local maxima/minima to retrieve the individual SLs (Fig. 3A). At the same time, the SL variability was significantly larger in the ANEPPS *vs* SHG measurements (Fig. 3B) regardless the use of local maxima or minima to index SL positions.

It should be noted as a side observation in this study that using Z-stacks in SHG measurements allows for a more precise evaluation of the 3D structure of the sarcomeric A-band geometry than can be obtained using ANEPPS imaging. For example, we implemented Z-stacks in some of our SHG measurements and found that an A-band regularity pattern exists in most of Z-planes (Fig. 4A) with the SL distribution characteristics to be non-discriminate between slices. The local peaks of the A-band regularity pattern revealed a high persistence in their physical positions along the longitudinal axis of the cell in the Z-direction, that is along the depth of the cell (Fig. 4B). In other words, some parts of the cell showed minor transversal changes (~0.5 μm, roughly one fourth of the sarcomere, for nearly the full depth of the cardiomyocyte) in the longitudinal positions of A-bands. This may indicate the presence of some functional role for transversal A-band geometry. Quantification of the shifts in the X-

position of each individual A-band when slicing across the cell depth, may allow for the measurement of such transversal changes. The middle frame in a Z-stack can be used as the referent to evaluate such shifts in the other frames (Fig. 4C). The more aligned A-bands are in Z-direction, the smaller a positional shift is observed. Therefore, SHG measurements may be helpful in the precise 3D imaging and reconstruction of the A-band “skeleton” as well as in the analysis of A-band (mis)alignment within a whole cell.

DISCUSSION

The main finding of our study is that the method of optical measurement is critical for proper characterization of individual sarcomere length (SL) variability, while it does not affect the measured average SL. In the present study, we implemented two optical measurement modalities: second-harmonic generation microscopy (SHG) and confocal two-photon imaging of fluorescent membrane-specific dye (ANEPPS). The first method marks the individual positions of A-bands that are purely internal structures of the sarcomere (Garcia-Canadilla et al., 2014; Zhao et al., 2019; Varga et al., 2020), while the second method visualizes the t-tubular striation pattern known to be closely aligned to sarcomeric Z-disks (Bub et al., 2010; Aguirre et al., 2014; Guo and Song, 2014), but which is not actually part of the sarcomere (Setterberg et al., 2021). The determination of averaged SL was shown to be insensitive to these optical methods confirming that a proper averaged value of SL can be obtained using fluorescent staining of t-tubules component of the sarcolemma. However, for subtle purposes such as the analysis of SL variability, the two methods were found not to be equivalent. In our study, the use of ANEPPS dye for sarcomeric visualization resulted in higher SL variability as compared to SHG microscopy that makes visible the central part of sarcomere. This could be due to a different extent of variability of the positions of A-bands versus t-tubules in each myocyte. The peak optical density of the t-tubule is somewhat aligned to the physical “center” of the Z-disk, but its actual peak position could be misaligned to some extent with the Z-disk center because a t-tubule is not physically part of the sarcomere (the “sloppy” coupling of t-tubules to the sarcomere Z-disks). In contrast, the A-band is the core inner component of the sarcomere and, therefore, its optical position should strongly follow the actual position of the “center” of the sarcomere. Our result therefore supports that SHG-based sarcomeric A-band visualization is the “gold standard” for

accurate analysis of individual SLs. It should be noted that in some of our SHG images we observed, like in previous reports (Recher et al., 2009; Varga et al., 2020), a double-banded signal in the A-bands of the sarcomere; in our analysis we avoided selection of myofibrils with such striation pattern.

A further question remains whether spatial resolution is a crucial factor that affects the precision of SL determination. In the present study we used the same spatial resolution as in our recent study on guinea pig myocytes, where we used transmitted light (TL) mode to acquire cell images (Lookin et al., 2022), and average SL was only nominally affected by the method of optical measurement – SHG, ANEPPS or TL; in the latter mode we found a slightly higher resting SL (data not shown), but this may be related to the absence of fluorescent dye in these cells. However, the use of SHG provided two-fold lower measured SL variability as compared to both ANEPPS (and TL in the paper cited above), despite equivalent spatial resolution of the optical systems. In the TL mode, the measured image is non-confocal and the sarcomeric striation derives from all myofibers along the cell depth. Therefore, imaging by conventional microscopy has inherently higher inconsistencies in the determination of an individual SL compared to confocal or SHG microscopy (Telley et al., 2006; Kobirumaki-Shimozawa et al., 2016). On the other hand, if the focal plane is properly chosen and optical phase-contrasting is used, the TL image may be as good for the SL analysis as the ANEPPS image, similar to previously reported data (Nance et al., 2015). Another reason of that non-confocal TL imaging may yield similar results as the ANEPPS confocal images is an axial regular alignment of sarcomeric structures (i.e. along the Z-axes) of the cardiomyocyte as we observed in the present study (cf. Fig 4). The structural basis for this regularity is not known and was not the focus of the currently study but, as an interesting side note, this regularity may also be expected to contribute to axial stiffness of a non-contracting

relaxed cardiomyocyte (Peyronnet et al., 2022). Therefore, quantitative measures of SL variability appear to be sensitive to the selection of which sarcomeric (related) structure is visualized, rather than the selection of optical method *per se* (fluorescent or transmitted light microscopy, confocal or brightfield microscopy).

The application of SHG microscopy can be further extended to the actively contracting cardiomyocytes and, especially, for the conditions where the myocyte is subjected to the physiological pre- or afterload. In our previous paper (Lookin et al., 2022) we reported that myocyte electrical activation increased SL variability as compared to the inactive state, concomitant with a reduction in overall SL. This result conformed to previously reported differences between relaxed and activated states in skeletal muscle (Moo et al., 2017; Moo and Herzog, 2018; Johnston et al., 2019; de Souza Leite and Rassier, 2020). However, an effect of sarcomere pre-stretch on SL variability in contracting cardiomyocytes remains to be determined. To elucidate this aspect in detail, SL variability in cardiomyocytes should be assessed with use of SHG microscopy as a prospective tool in the determination of individual sarcomeres, in addition to the widely used fluorescent staining.

In conclusion, we found that the method of optical measurement is critical for proper characterization of individual sarcomere length (SL) variability, while it does not affect the measured average SL. Our results, therefore, support the notion that SHG-based sarcomeric A-band visualization forms the “gold standard” for precise analysis of individual sarcomeres.

ACKNOWLEDGEMENTS

We thank Patrice Bideaux for assistance with the rat cell isolation procedures.

AUTHOR CONTRIBUTIONS

OL, PdT, NB and OC contributed to the conception of the study, design of experiments, analysis, and interpretation of the results. PdT, NB, CG, TC and OC contributed to the experimental measurements. CG and TC provided technical assistance in SHG measurements. OL made software for data processing. The manuscript was written by OL, PdT and OC. All authors approved the final version of the manuscript.

FUNDING

The study was supported by the Centre national de la recherche scientifique (France, grant #IEA00401 to OC), and NIH (HL62426 to PdT).

FIGURE LEGENDS

Figure 1. Representative confocal images of an isolated cardiomyocyte obtained by second-harmonic generation microscopy (SHG) and by membrane fluorescent staining with di-4-ANEPPS (ANEPPS). (A) SHG (top) and ANEPPS (bottom) images with five regions of interest (ROI) as indicated (colored lines) following the paths of single myofibrils. The insets show the sarcomeric striation of a single ROI (cf. yellow arrows). (B) Sarcomere striation profiles taken from a single ROI using SHG and ANEPPS images. The arrows show the positions of local maxima in the intensity profiles (note their relative shift by a half sarcomere because SHG visualizes the center of sarcomeres, while ANEPPS visualizes the areas near the sarcomeric Z-disks).

Figure 2. The average sarcomere length (SL) value, but not the SL variability, is independent of the optical method used to derive SL striations. Confocal measurements were made either by using second-harmonic generation microscopy (SHG), or by fluorescent membrane staining with di-4-ANEPPS (ANEPPS) in n = 26 isolated cardiomyocytes from N = 3 hearts. The median SL value (A) and the following absolute and relative quantitative measures of SL variability were analyzed: (B) Inter-quartile range (IQR), (C) Median absolute deviation (MAD), (D) IQR divided by median SL, and (E) MAD divided by median SL. The data in panels (A-E) are shown as mean ± S.D. Differences between SHG and ANEPPS were significant at $p < 0.0001$ (Wilcoxon matched-pairs signed rank test). (F) Averaged distribution plots for individual SL values obtained by SHG or ANEPPS. The peaks of the plots correspond to averaged median SL, and the distributions are shown as a % of the corresponding median SL.

Figure 3. The use of either local maxima (max) or local minima (min) of the sarcomere striation profile generates non-discriminated quantitative measures of sarcomere length (SL) median value and the variability in the individual SLs. Confocal measurements were by second-harmonic generation microscopy (SHG) or by fluorescent membrane staining with di-4-ANEPPS (ANEPPS) in n = 26 isolated cardiomyocytes from N = 3 hearts. (A) Median SL, (B) Median absolute deviation (MAD) divided by median SL (MADM). Differences between SHG(max) and SHG(min) or between ANEPPS(max) and ANEPPS(min) were not significant (Wilcoxon matched-pairs signed rank test).

Figure 4. The applicability of SHG measurements for evaluation of sarcomeric A-band 3D-structure. (A) A series of five SHG images of A-bands in an isolated cardiomyocyte obtained at different positions along the Z-axis, i.e. from the top (frame #1) to the bottom of the cell (frame #5). The yellow-colored ROI on each frame is kept fixed in size and X/Y-positions and used to retrieve A-band axial regularity. Scale bar on the top image is common for all images. (B) Curves of A-band regularity patterns obtained from the corresponding ROIs shown in the images in panel (A). (C) The shifts of individual A-band X-position across the slices as calculated relative to the X-position in the "center of the cell" (i.e. frame #3). The plots are obtained for four frames (two below and two above the middle frame). The magnitude of the longitudinal shifts, their variation along the X-axis, and the actual direction of the change during the axial slicing across the cell depth may be used to estimate Z-axis A-band (mis)alignment.

REFERENCES

Adkins, A.N., R.M. Fong, J.P.A. Dewald, and W.M. Murray. 2022. Variability of in vivo sarcomere length measures in the upper limb obtained with second harmonic generation microendoscopy. *Front Physiol*. 12:817334. https://doi.org/10.3389/fphys.2021.817334

Aguirre, A.D., C. Vinegoni, A. Sebas, and R. Weissleder. 2014. Intravital imaging of cardiac function at the single-cell level. *PNAS.* 111(31):11257-11262. https://doi.org/10.1073/pnas.1401316111

Andre L, Boissière J, Reboul C, Perrier R, Zalvidea S, Meyer G, Thireau J, Tanguy S, Bideaux P, Maurice Hayot M, François Boucher F, Philippe Obert P, Olivier Cazorla O, Sylvain Richard S. 2010. Carbon monoxide pollution aggravates ischemic heart failure through oxidative stress pathway. *Am J Respir Crit Care Med* 181(6):587-595. https://doi.org/10.1164/rccm.200905-0794OC

Botcherby, E.J., A. Corbett, R.A.B. Burton, C.W. Smith, C. Bollensdorff, M.J. Booth, P. Kohl, T. Wilson, and G. Bub. 2013. Fast measurement of sarcomere length and cell orientation in langendorff-perfused hearts using remote focusing microscopy. *Circ Res*. 113:863-870. https://doi.org/10.1161/CIRCRESAHA.113.301704

Bub, G., P. Camelliti, C. Bollensdorff, D.J. Stuckey, G. Picton, R.A.B. Burton, K. Clarke, and P. Kohl. 2010. Measurement and analysis of sarcomere length in rat cardiomyocytes in situ and in vitro. *Am J Physiol Heart Circ Physiol.* 298:H1616-H1625. https://doi.org/10.1152/ajpheart.00481.2009

Buttgereit, A. 2017. Second harmonic generation microscopy of muscle cell morphology and dynamics. *Methods Mol Biol.* 1601:229-241. https://doi.org/10.1007/978-1-4939-6960-9_18

de Souza Leite, F., F.C. Minozzo, D. Altman, and D.E. Rassier. 2017. Microfluidic perfusion shows intersarcomere dynamics within single skeletal muscle myofibrils. *Proc Natl Acad Sci U S A.* 114(33):8794-8799. https://doi.org/10.1073/pnas.1700615114

de Souza Leite, F., and D.E. Rassier. 2020. Sarcomere length nonuniformity and force regulation in myofibrils and sarcomeres. *Biophys J.* 119:1-6. https://doi.org/10.1016/j.bpj.2020.11.005

de Tombe, P.P., and H.E.D.J. ter Keurs. 2016. Cardiac muscle mechanics: sarcomere length matters. *J Mol Cell Cardiol.* 91:148-150. https://doi.org/10.1016/j.yjmcc.2015.12.006

Dobesh, D.P., J.P. Konhilas, and P.P. de Tombe. 2002. Cooperative activation in cardiac muscle: impact of sarcomere length. *Am J Physiol Heart Circ Physiol.* 282:H1055-H1062. https://doi.org/10.1152/ajpheart.00667.2001

Dowrick, J.M., A.J. Anderson, M.L. Cheuk, K. Tran, P.M.F. Nielsen, J.-C. Han, and A.J. Taberner. 2021. Simultaneous brightfield, fluorescence, and optical coherence tomographic imaging of contracting cardiac trabeculae ex vivo. *J Vis Exp.* 176. https://doi.org/10.3791/62799

Garcia-Canadilla, P., A. Gonzalez-Tendero, I. Iruretagoyena, F. Crispi, I. Torre, I. Amat-Roldan, B.H. Bijnens, and E. Gratacos. 2014. Automated cardiac sarcomere analysis from second harmonic generation images. *J Biomed Opt.* 19(5):056010. https://doi.org/10.1117/1.JBO.19.5.056010

Guo, A., and L.-S. Song. 2014. AutoTT: automated detection and analysis of T-tubule architecture in cardiomyocytes. *Biophys J.* 106(12):2729-2736. https://doi.org/10.1016/j.bpj.2014.05.013

Haeger, R., F. de Souza Leite, and D.E. Rassier. 2020. Sarcomere length nonuniformities dictate force production along the descending limb of the force–length relation. *Proc R Soc B.* 287:20202133. https://doi.org/10.1098/rspb.2020.2133

Haeger, R.M., and D.E. Rassier. 2020. Force enhancement after stretch of isolated myofibrils is increased by sarcomere length non-uniformities. *Sci Rep*. 10:21590. https://doi.org/10.1038/s41598-020-78457-1

Herzog, W. 2022. What can we learn from single sarcomere and myofibril preparations? *Front Physiol*. 13:837611. https://doi.org/10.3389/fphys.2022.837611

Homan, T., H. Delanoë-Ayari, A.C. Meli, O. Cazorla, C. Gergely, A. Mejat, P. Chevalier, and A. Moreau. 2021. MorphoScript: a dedicated analysis to assess the morphology and contractile structures of cardiomyocytes derived from stem cells. *Bioinformatics.* btab400. https://doi.org/10.1093/bioinformatics/btab400

Johnston, K., A. Jinha, and W. Herzog. 2016. The role of sarcomere length non-uniformities in residual force enhancement of skeletal muscle myofibrils. *R Soc Open Sci.* 3:150657. https://doi.org/10.1098/rsos.150657

Johnston, K., E.K. Moo, A. Jinha, and W. Herzog. 2019. On sarcomere length stability during isometric contractions before and after active stretching. *J Exp Biol.* 222:jeb209924. https://doi.org/10.1242/jeb.209924

Kobirumaki-Shimozawa, F., K. Oyama, T. Shimozawa, A. Mizuno, T. Ohki, T. Terui, S. Minamisawa, S. Ishiwata, and N. Fukuda. 2016. Nano-imaging of the beating mouse heart in vivo: Importance of sarcomere dynamics, as opposed to sarcomere length per se, in the regulation of cardiac function. *J Gen Physiol.* 147(1):53-62. https://doi.org/10.1085/jgp.201511484

Kobirumaki-Shimozawa, F., T. Shimozawa, K. Oyama, Y. Kushida, T. Terui, S. Ishiwata, and N. Fukuda. 2018. Optimization of fluorescent labeling for in vivo nanoimaging of sarcomeres in the mouse heart. *BioMed Res Intl.* 2018:4349170. https://doi.org/10.1155/2018/4349170

Lookin, O., A. Khokhlova, T. Myachina, X. Butova, O. Cazorla, and P. de Tombe. 2022. Contractile state dependent sarcomere length variability in isolated guinea-pig cardiomyocytes. *Front Physiol.* 13:857471. https://doi.org/10.3389/fphys.2022.857471

Moo, E.K., and W. Herzog. 2018. Single sarcomere contraction dynamics in a whole muscle. *Sci Rep.* 8:15235. https://doi.org/10.1038/s41598-018-33658-7

Moo, E.K., T.R. Leonard, and W. Herzog. 2017. In vivo sarcomere lengths become more non-uniform upon activation in intact whole muscle. *Front Physiol.* 8:1015. https://doi.org/10.3389/fphys.2017.01015

Nance, M.E., J.T. Whitfield, Y. Zhu, A.K. Gibson, L.M. Hanft, K.S. Campbell, G.A. Meininger, K.S. McDonald, S.S. Segal, and T.L. Domeier. 2015. Attenuated sarcomere lengthening of the aged murine left ventricle observed using two-photon fluorescence microscopy. *Am J Physiol Heart Circ Physiol.* 309:H918-H925. https://doi.org/10.1152/ajpheart.00315.2015

Pasqualin, C., F. Gannier, A. Yu, C.O. Malécot, P. Bredeloux, and V. Maupoil. 2016. SarcOptiM for ImageJ: high-frequency online sarcomere length computing on stimulated cardiomyocytes. *Am J Physiol Cell Physiol.* 311:C277-C283. https://doi.org/10.1152/ajpcell.00094.2016

Peyronnet R, Desai A, Edelmann JC, Cameron BA, Emig R, Kohl P, Dean D. 2022. Simultaneous assessment of radial and axial myocyte mechanics by combining atomic force microscopy and carbon fibre techniques. *Philos Trans R Soc Lond B Biol Sci.* 377(1864):20210326. https://doi.org/10.1098/rstb.2021.0326.

Plotnikov SV, Millard AC, Campagnola PJ, Mohler WA. 2006. Characterization of the myosin-based source for second-harmonic generation from muscle sarcomeres. *Biophys J*. 2006 90(2):693-703. https://doi.org/ 10.1529/biophysj.105.071555.

Rassier, D.E. 2017 Sarcomere mechanics in striated muscles: from molecules to sarcomeres to cells. *Am J Physiol Cell Physiol.* 313(2):C134-C145. https://doi.org/10.1152/ajpcell.00050.2017

Recher, G., D. Rouède, P. Richard, A. Simon, J.-J. Bellanger, and F. Tiaho. 2009. Three distinct sarcomeric patterns of skeletal muscle revealed by SHG and TPEF microscopy. *Opt Express.* 17(22):19763-19777. https://doi.org/10.1364/OE.17.019763

Setterberg, I.E., C. Le, M. Frisk, J. Li, and W.E. Louch. 2021. The physiology and pathophysiology of t-tubules in the heart. *Front Physiol.* 12:718404. https://doi.org/10.3389/fphys.2021.718404

Shintani, S.A., K. Oyama, F. Kobirumaki-Shimozawa, T. Ohki, S. Ishiwata, and N. Fukuda. 2014. Sarcomere length nanometry in rat neonatal cardiomyocytes expressed with a-actinin-AcGFP in Z discs. *J Gen Physiol.* 143:513-524. https://doi.org/10.1085/jgp.201311118

Telley, I.A., J. Denoth, E. Stussi, G. Pfitzer, and R. Stehle. 2006. Half-sarcomere dynamics in myofibrils during activation and relaxation studied by tracking fluorescent markers. *Biophys J.* 90:514-530. https://doi.org/10.1529/biophysj.105.070334

Tsukamoto, S., T. Fujii, K. Oyama, S.A. Shintani, T. Shimozawa, F. Kobirumaki-Shimozawa, S. Ishiwata, and N. Fukuda. 2016. Simultaneous imaging of local calcium and single sarcomere length in rat neonatal cardiomyocytes using yellow Cameleon-Nano140. *J Gen Physiol.* 148(4):341-355. https://doi.org/10.1085/jgp.201611604

Varga, B., A.C. Meli, S. Radoslavova, M. Panel, A. Lacampagne, C. Gergely, O. Cazorla, and T. Cloitre. 2020. Internal structure and remodeling in dystrophin-deficient

cardiomyocytes using second harmonic generation. *Nanomedicine.* 30:102295. https://doi.org/10.1016/j.nano.2020.102295

Wagner, E., S. Brandenburg, T. Kohl, and S.E. Lehnart. 2014. Analysis of tubular membrane networks in cardiac myocytes from atria and ventricles. *J Vis Exp.* 92:e51823. https://doi.org/10.3791/51823

Yue, X., R. Zhang, B. Kim, A. Ma, K.D. Philipson, and J.I. Goldhaber. 2017. Heterogeneity of transverse-axial tubule system in mouse atria: Remodeling in atrial-specific Na+–Ca2+ exchanger knockout mice. *J Mol Cell Cardiol.* 108:50-60. https://doi.org/10.1016/j.yjmcc.2017.05.008

Zhao, H., R. Cisek, A. Karunendiran, D. Tokarz, B.A. Stewart, and V. Barzda. 2019. Live imaging of contracting muscles with wide-field second harmonic generation microscopy using a high power laser. *Biomed Opt Express.* 10(10):5130-5135. https://doi.org/10.1364/BOE.10.005130

A

SHG

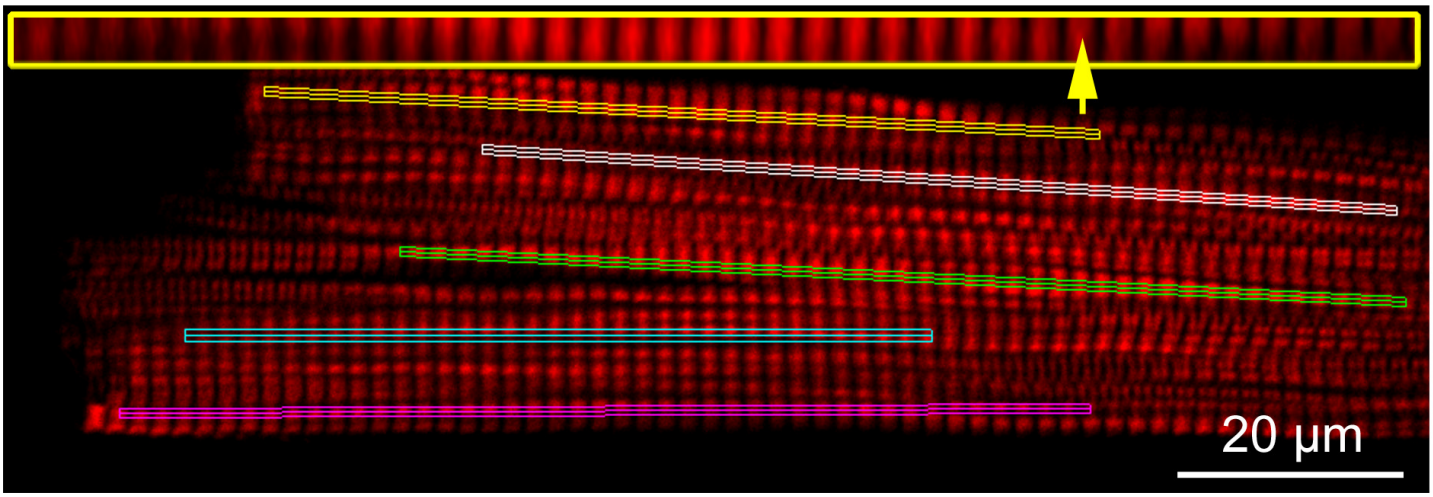

ANEPPS

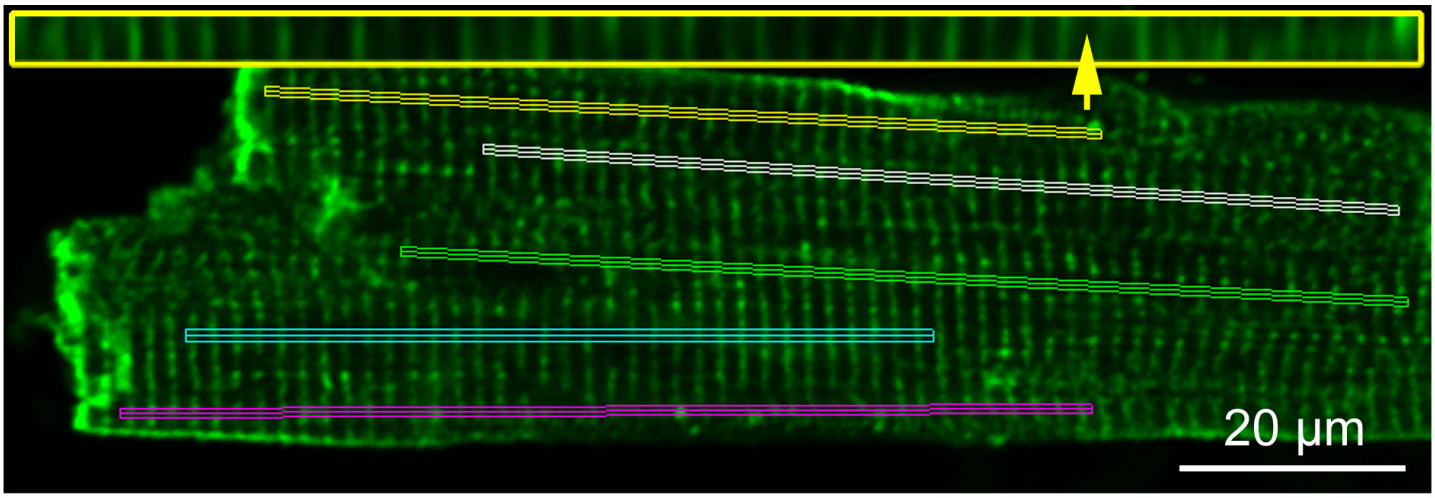

B

SHG

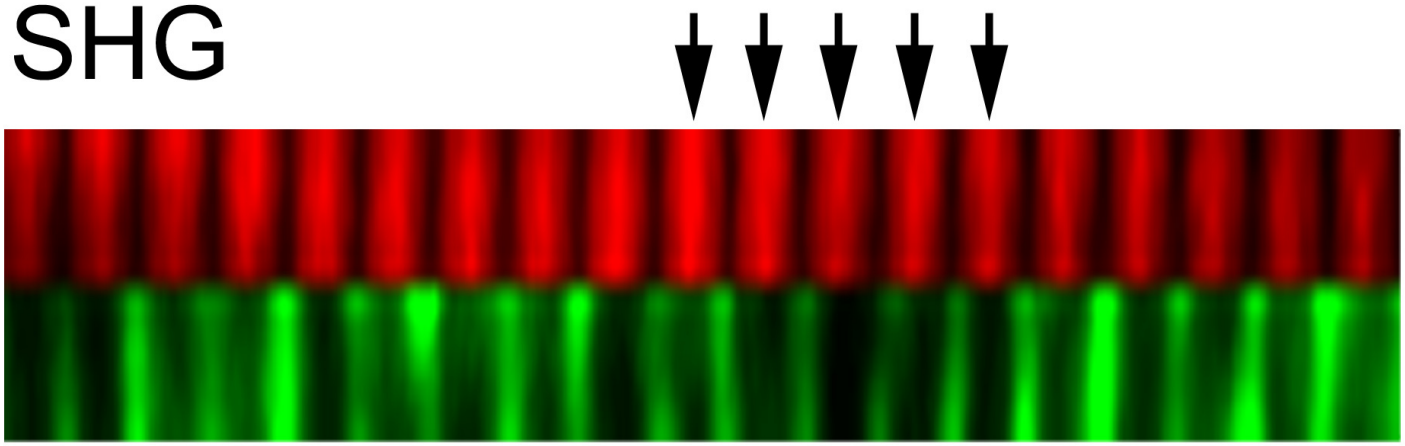

ANEPPS

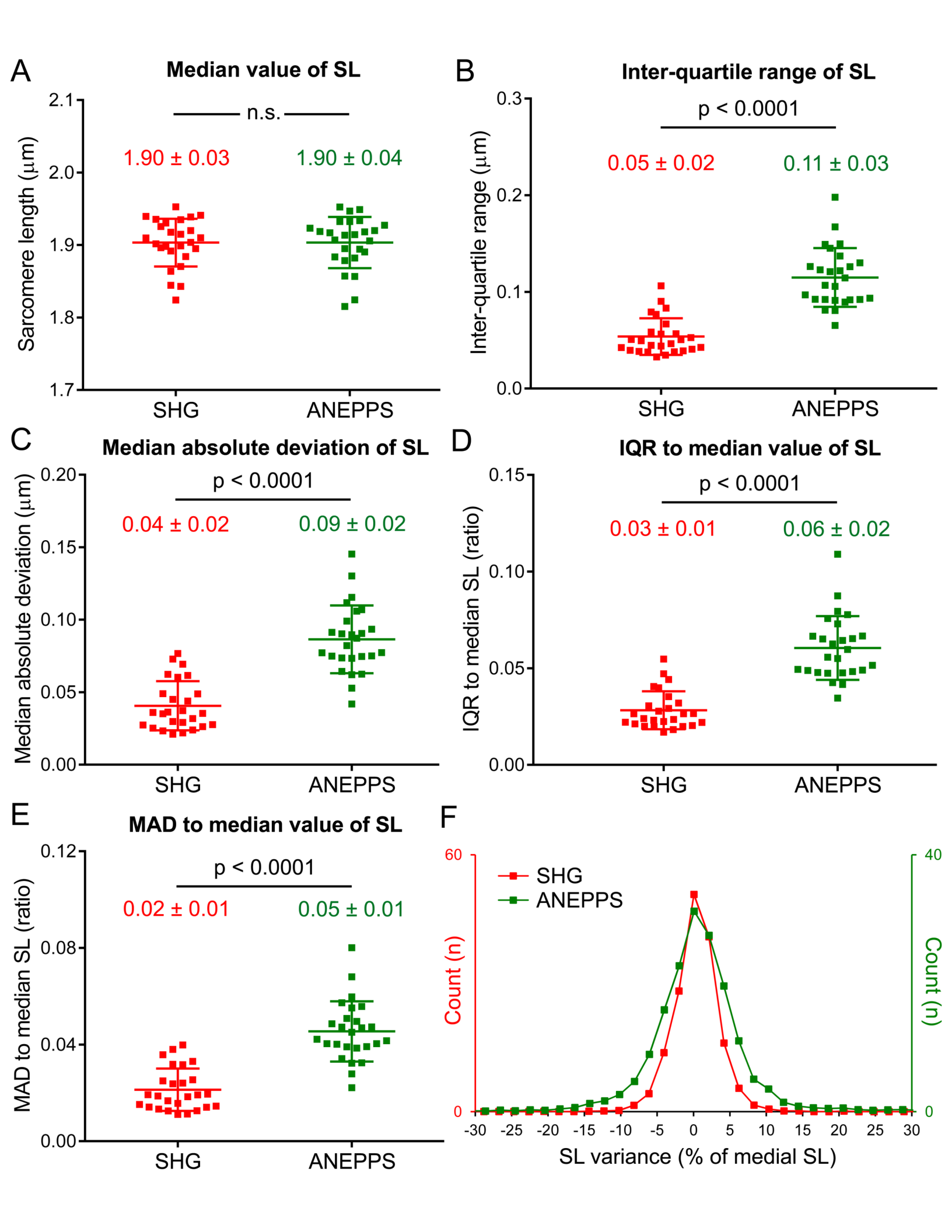
A
Median value of SL
n.s.
1.90 ± 0.03
1.90 ± 0.04
Sarcomere length (μm)
2.1
2.0
1.9
1.8
1.7
SHG
ANEPPS
B
Inter-quartile range of SL
p < 0.0001
0.05 ± 0.02
0.11 ± 0.03
Inter-quartile range (μm)
0.3
0.2
0.1
0.0
SHG
ANEPPS
C
Median absolute deviation of SL
p < 0.0001
0.04 ± 0.02
0.09 ± 0.02
Median absolute deviation (μm)
0.20
0.15
0.10
0.05
0.00
SHG
ANEPPS
D
IQR to median value of SL
p < 0.0001
0.03 ± 0.01
0.06 ± 0.02
IQR to median SL (ratio)
0.15
0.10
0.05
0.00
SHG
ANEPPS
E
MAD to median value of SL
p < 0.0001
0.02 ± 0.01
0.05 ± 0.01
MAD to median SL (ratio)
0.12
0.08
0.04
0.00
SHG
ANEPPS
F
SHG
ANEPPS
Count (n)
60
0
Count (n)
40
0
-30 -25 -20 -15 -10 -5 0 5 10 15 20 25 30
SL variance (% of medial SL)

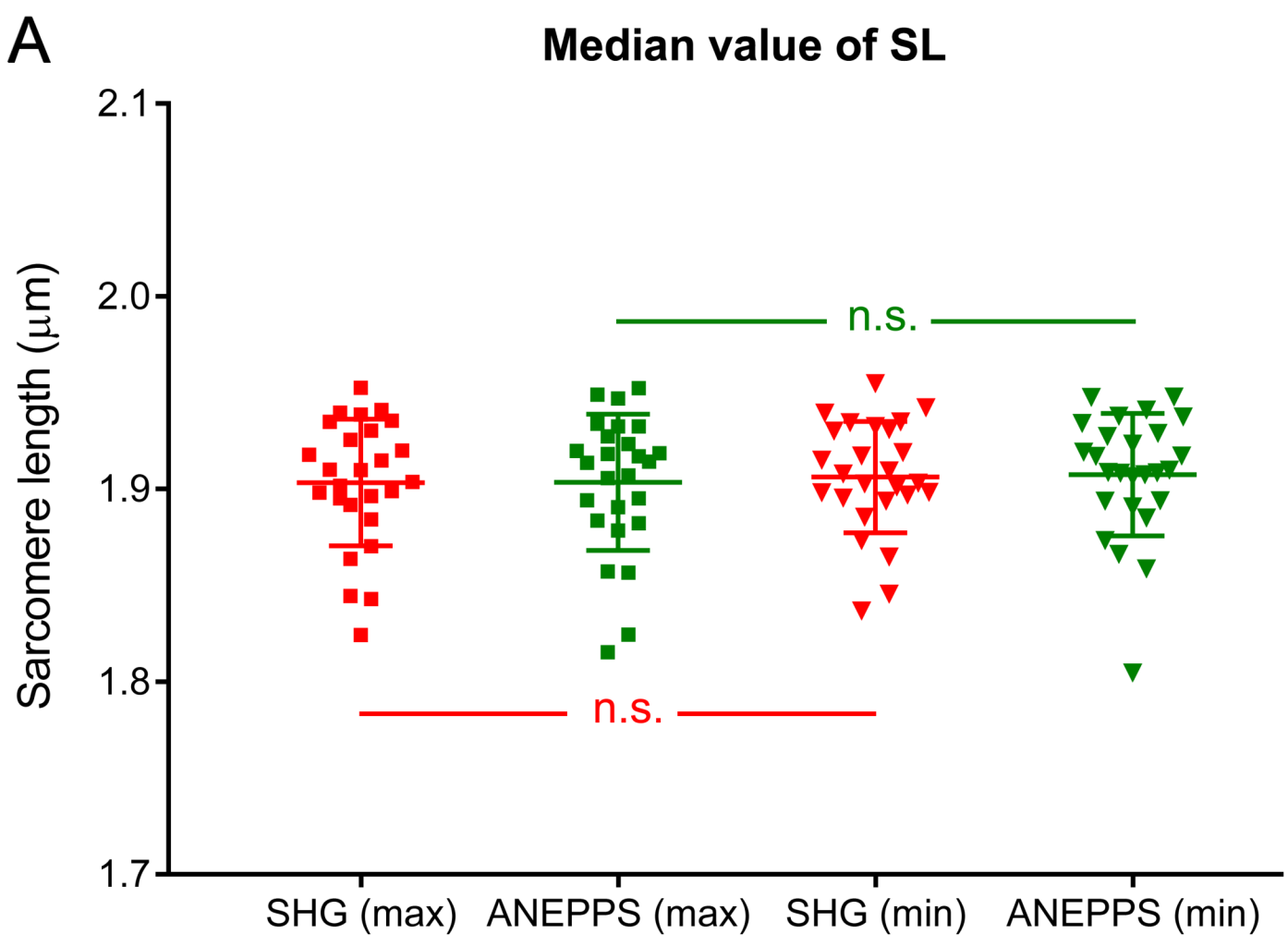
A
Median value of SL
Sarcomere length (μm)
2.1
2.0
1.9
1.8
1.7
n.s.
n.s.
SHG (max)
ANEPPS (max)
SHG (min)
ANEPPS (min)

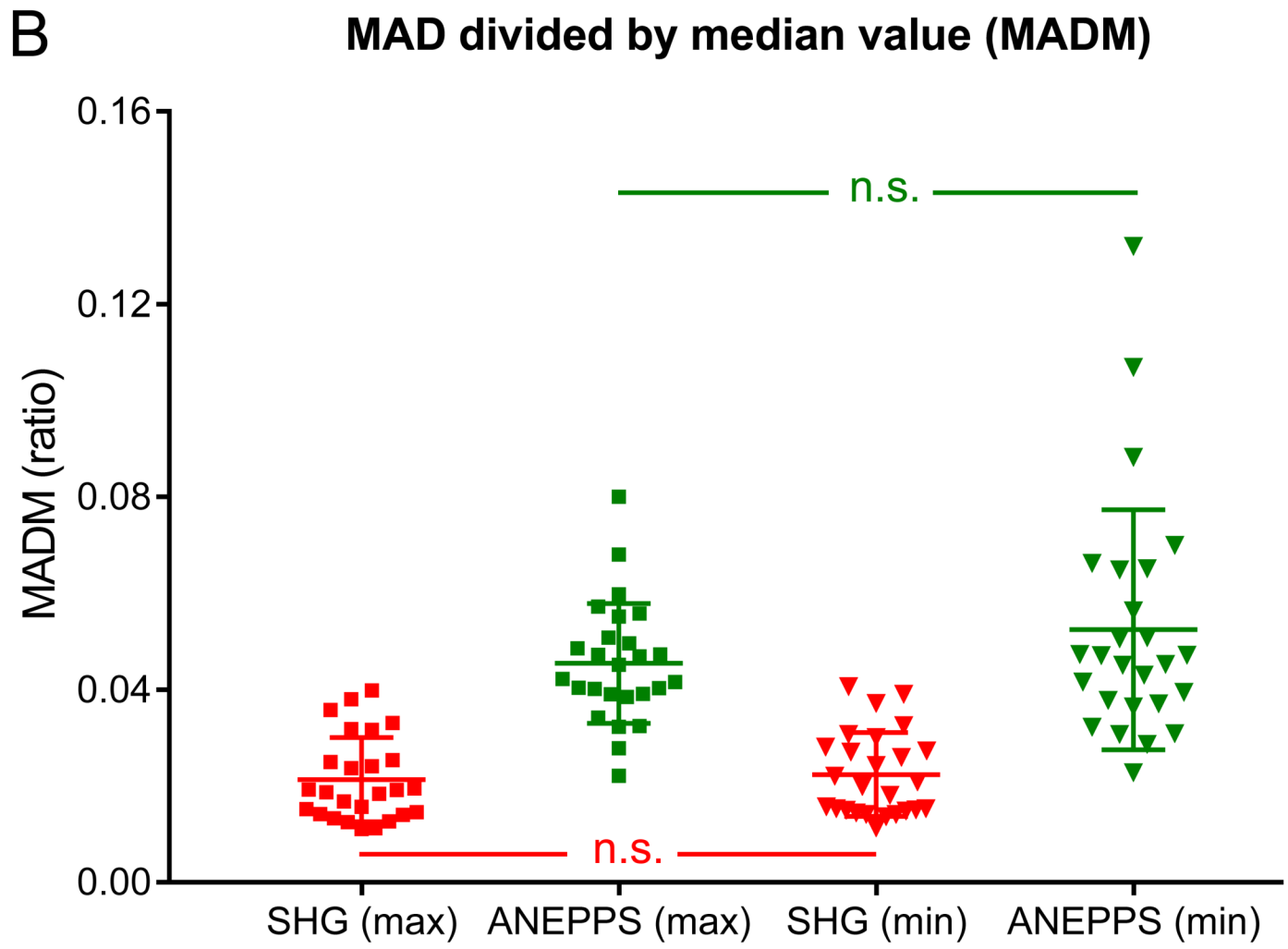
B
MAD divided by median value (MADM)
MADM (ratio)
0.16
0.12
0.08
0.04
0.00
n.s.
n.s.
SHG (max)
ANEPPS (max)
SHG (min)
ANEPPS (min)

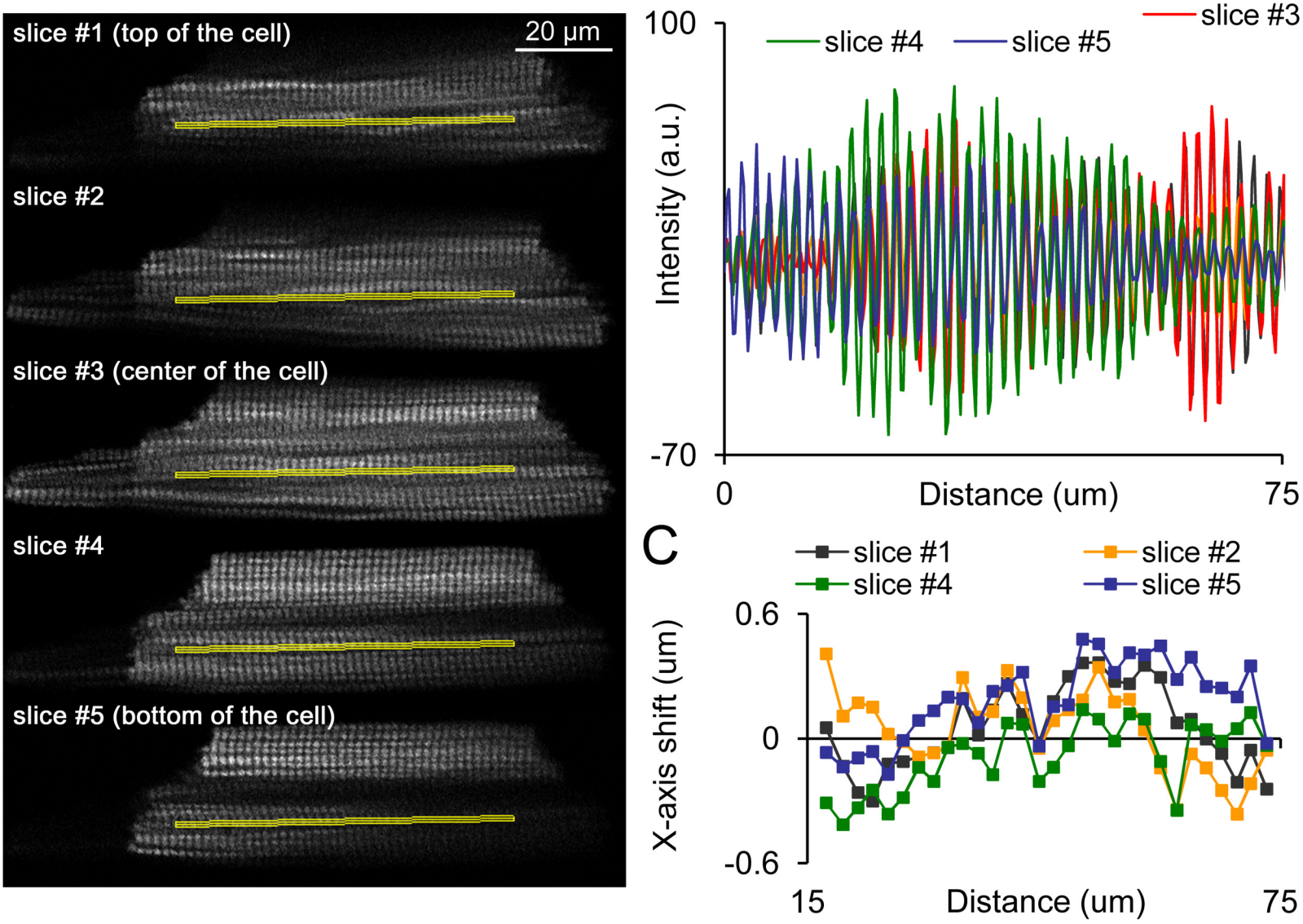
A
slice #1 (top of the cell)
20 μm
slice #2
slice #3 (center of the cell)
slice #4
slice #5 (bottom of the cell)
B
slice #1
slice #2
slice #3
slice #4
slice #5
100
-70
Intensity (a.u.)
0
Distance (um)
75
C
slice #1
slice #2
slice #4
slice #5
0.6
0
-0.6
X-axis shift (um)
15
Distance (um)
75